Journal of Molecular Liquids 314 (2020) 113588

Contents lists available at ScienceDirect

Journal of Molecular Liquids

journal homepage: www.elsevier.com/locate/molliq

Tuning of metal oxides photocatalytic performance using Ag nanoparticles integration

Hassan Karimi-Maleh [a,b,c,*], Baskaran Ganesh Kumar [d,e,**], Saravanan Rajendran [f,***], Jiaqian Qin [g], S. Vadivel [h], D. Durgalakshmi [i], F. Gracia [j], Matias Soto-Moscoso [k], Yasin Orooji [l,m], Fatemeh Karimi [n,o,****]

[a] School of Resources and Environment, University of Electronic Science and Technology of China, P.O. Box 611731, Xiyuan Ave, Chengdu, PR China
[b] Department of Chemical Engineering, Quchan University of Technology, Quchan, Iran
[c] Department of Chemical Sciences, University of Johannesburg, P.O. Box 17011, Doornfontein Campus, 2028 Johannesburg, South Africa
[d] Department of Chemistry, PSR Arts and Science College (affiliated to Madurai Kamaraj University), Sivakasi, Tamil Nadu, India
[e] Department of Science and Humanities, PSR Engineering college (affiliated to Anna University), Sivakasi, Tamil Nadu, India
[f] Faculty of Engineering, Department of Mechanical Engineering, University of Tarapaca, Avda. General Velasquez, 1775 Arica, Chile
[g] Research Unit of Advanced Materials for Energy Storage, Metallurgy and Materials Science Research Institute, Chulalongkorn University, Bangkok 10330, Thailand
[h] Department of Chemistry, PSG College of Technology, Coimbatore 641004, India
[i] Department of Medical Physics, Anna University, Chennai 600 025, India
[j] Department of Chemical Engineering, Biotechnology and Materials, University of Chile, Beauchef 851, 6th Floor, Santiago, Chile
[k] Departamento de Física, Facultad de Ciencias, Universidad del Bío-bío, Avenida Collao 1202, Casilla 15-C, Concepción, Chile
[l] Co-Innovation Center of Efficient Processing and Utilization of Forest Resources, Nanjing Forestry University, Nanjing 210037, China
[m] College of Materials Science and Engineering, Nanjing Forestry University, Nanjing 210037, PR China
[n] Nanostructure Based Biosensors Research Group, Ton Duc Thang University, Ho Chi Minh City, Vietnam
[o] Faculty of Applied Sciences, Ton Duc Thang University, Ho Chi Minh City, Vietnam

ARTICLE INFO

Article history:
Received 30 January 2020
Received in revised form 16 May 2020
Accepted 11 June 2020
Available online 15 June 2020

Keywords:
Nanomaterial
Photocatalysis
Metal oxide
Dye degradation
Water purification

ABSTRACT

Water contamination is increasingly an important issue in developing and under developed countries. The main cause of water contaminations are industrial dyes and toxic chemicals. Hence many technologies are being developed to de-contaminate the toxic materials. The photocatalytic de-contamination of dyes is an effective and simple technology to purify water. Among various photocatalysts, the transition metal based oxides (TiO_2, NiO and ZnO) being the state-of art photocatalytic material. But, the metal oxides have large band gap and suffers from the fact that it predominantly absorbs the Ultra Violet region of irradiation. But, any viable photocatalytic technology demands absorption in the visible light region, so as to utilize the cost-free sun light. Herein, we tune and utilize the metal oxides through the integration of Ag metal nanoparticles. The synthesized materials were completely analyzed by PXRD, HRTEM, UV, XPS and BET instruments. All TiO_2/Ag, NiO/Ag and ZnO/Ag nanocomposites were subjected to photocatalytic degradation using visible light. The nanocomposites acted as photocatalyst and degrade the colorful methyl orange and colorless toxic 4-chlorophenol. Among the aforementioned three samples, TiO_2/Ag exhibited best performance than ZnO/Ag and NiO/Ag. We attributed the enhancement of photocatalytic activity due to Plasmons assistance and nanoscale regime of photocatalyst. In summary, we tuned the metal oxide photocatalytic performance using the Ag nanoparticle surface Plasmon resonance.

* Correspondence to: H. K.-Maleh, School of Resources and Environment, University of Electronic Science and Technology of China, P.O. Box 611731, Xiyuan Ave, Chengdu, PR China.
** Correspondence to: B. G. Kumar, Department of Chemistry, PSR Arts and Science College (affiliated to Madurai Kamaraj University), Sivakasi, Tamil Nadu, India.
*** Correspondence to Saravanan Rajendran, Faculty of Engineering, Department of Mechanical Engineering, University of Tarapaca, Avda. General Velasquez, 1775 Arica, Chile
**** Correspondence to: F. Karimi, Nanostructure Based Biosensors Research Group, Ton Duc Thang University, Ho Chi Minh City, Vietnam.
E-mail addresses: hassan@uestc.edu.cn (H. Karimi-Maleh), suviganu@gmail.com (B.G. Kumar), saravanan3.raj@gmail.com (S. Rajendran), fatemeh.karimi@tdtu.edu.vn (F. Karimi).

https://doi.org/10.1016/j.molliq.2020.113588
0167-7322/

1. Introduction

The water sources contain various types of contamination including biological contamination (pathogens-virus and bacteria) and chemical contamination (industrial waste and pesticides) [1–3]. Among these contaminants, biological contamination is less involved in water pollution because most of them can be removed by simple heating [4,5]. Hence, the chemical contaminants gained much attention in environmental pollution and should be removed from water [6,7]. The growing industrial evolution elevates the level of contaminants which leads to increased risk of serious diseases in children including gastrointestinal disorder, learning disorders, endocrine hormonal disruption, and uncontrollable cancer [8,9]. More than 75% of all diseases are affected to humans due to poor water quality. Hence the contaminants must be identified and removed from the water. The most common chemical contaminants found in waters are the industrial discharge, dyes, pesticides, drugs and cosmetics [10]. Since chemical contaminants are the real concern to the society, many technologies and strategies are being developed through-out the world to provide novel solution [11]. Among the various technologies, heterogenous photocatalysis is having a bright future [12–18]. The photocatalysis is green and clean photochemical method of water purification. In the photocatalytic process, the semiconductor converts photon energy into chemical oxidation/reduction process which will further degrade the contaminants in water through the free radical formation. As a result, the chemical contaminants are degraded by photochemical oxidation/reduction. Overall, the photocatalyst based water purification is promising and widely adopted due to its simplicity, cost, robustness, solar energy as input, effective with all types of contaminants and attractive efficiency [19].

Recently, appreciable efforts were focused on TiO_2 or ZnO based photocatalytic water purification and made substantial improvements in sustainable water purification. However, the metal oxides have intrinsically low efficiency due to poor absorption if light is in visible region. The metal oxides absorb in Ultra Violet region and absorb less in visible region (4%) due to band alignment (e.g. TiO_2 - 3.2 eV for anatase) [20]. The shifting absorption of photocatalysis from UV to visible light is important because the visible light is naturally abundant and can be cost-effective for water purification technology which was previously done by several nanocomposite systems. Nanomaterials and especially nanocomposites showed many advantages due to unique properties and high surface area [21–27]. The nanocomposite systems are used for various applications like solar cells, biosensors, antibacterial activity including photocatalytic activity [28–35]. In the recent times, the integration of noble metals with metal oxides also suppresses the charge recombination due to shift in fermi level [36]. The key absorption process of photocatalysis can be improved by several ways and one of the promising novel methods is plasmonic photocatalysis [37–43]. When the plasmonic materials integrate with metal oxides, the wide band gap of the semiconductor shifts to lower band gap and hence is in visible region. The phenomenon of surface Plasmons are the collective electrons and surface charges in the conductive materials which respond strongly with the light. The noble metals such as gold, platinum and silver nanoparticles show tunable Plasmon resonance in the visible light region [44]. Among that silver is desirable for plasmonic photocatalysis, because of its balanced stability and cost. Additionally, nano regime of the plasmonic particles provide more toxic chemicals adsorption on the surface. Silver nanoparticles supported metal oxides are expected to be novel plasmonic photocatalyst. Recently, Ag integrated plasmonic photocatalysts such as TiO_2/Ag [45], AgCl/Ag [46], Cu_2O/Ag [47] and ZnO/Ag [48,49] were reported. In each case, absorption has shifted to visible region and performance has been enhanced by Ag particles. Clearly, when compared to conventional metal oxides, Ag integrated metal oxides are expected to show increased performance through the surface Plasmons assistance.

Here, it has been demonstrated the preparation of Ag Plasmon enriched metal oxide nanoparticles. The ZnO/Ag, NiO/Ag and TiO_2/Ag nanocomposites were synthesized via solvothermal method. To analyze the proposed strategy, TiO_2, ZnO and NiO are chosen in which the wide band gap materials are known for the photocatalytic performance for 30 years and shifted the band gap to the visible region. The materials were completely characterized by PXRD, HRTEM, UV, BET and XPS analysis. The silver integration was established through the shift in the absorbance of metal oxides. The structural analysis showed that the integration was successful and Ag integration did not alter the crystal structure. Using the prepared photocatalysts, the degradation of colorful contaminant methyl orange and colorless 4-chlorophenol was carried. All Ag integrated metal oxides exhibited superior performance when compared to pure metal oxides. Among the three metal oxide composites, TiO_2/Ag exhibited best performance than ZnO/Ag and NiO/Ag. It is to be noted that the performance of ZnO/Ag has showed comparable performance with TiO_2/Ag. The NiO/Ag photocatalyst displayed the moderate degradation performance with both methyl orange and 4-chlorophenol. This enhancement of photocatalytic activity is due to Plasmon assistance and nanoscale of photocatalyst.

2. Experimental section

The following chemicals are purchased from Aldrich and utilized without purification. All the solutions are used with an analytical grade. The solvothermal method has been utilized to synthesize the photocatalyst.

2.1. Preparation of TiO_2/Ag nanocomposite

In this report, the TiO_2@Ag nanocomposite was synthesized by solvothermal method. Initially, 3 wt% of dissolved $AgNO_3$ (in a 10 ml of the distilled water) solution was mixed with 10 ml of titanium (IV) isopropoxide solution and 50 ml of 2-propanol was added into the above solution. Then 5 ml of acetic acid was added to the reaction flask for gel formation. Finally, the prepared gel was transfer to autoclave and calcined at 160 °C for 24 h along with the heating rate of 4°/min. After the reaction time, the reaction flask was cooled down to ambient temperature. The obtained precipitate was centrifuged and repeatedly purified with double distilled water and ethanol many times to discard any undesired by-products from the reaction. After purification, TiO_2/Ag nanocomposite powder was obtained. To remove the traces of water, the separated powder was evacuated at vacuum for 2 h before further analysis. The obtained nanoparticles were sensitive to light and air, the composite was stored in argon-filled glove box for long time use.

2.2. Preparation of ZnO/Ag composites

The ZnO/Ag nanocomposite was prepared via solvothermal method. ZnO@Ag nanomaterials was synthesized via solvo-hydrothermal method. Initially, 600 RPM stirring condition of 0.1 mol of sodium pellet was dissolved in 20 ml of water. On the other hand, 150 ml of ethanol, 0.2 g of citric acid, 3% wt of $AgNO_3$ were mixed with 2.6 g of zinc acetate in a beaker. The dissolved NaOH was mixed drop wise into the above prepared solution. The entire reaction mixture was stirred 2 h and transferred to autoclave and calcined at 160 °C for 24 h at a heating rate of 4°/min. The obtained precipitate was centrifuged and repeatedly purified with double distilled water and ethanol multiple times. Further, the material was evacuated at vacuum for 2 h, then finally obtained the ZnO@Ag nanomaterial.

2.3. Preparation of NiO/Ag composites

The NiO/Ag nanocomposite was synthesized through solvothermal method. Initially, for NiO@Ag preparation; nickel (II) nitrate was mixed with 150 ml of ethanol, 3 wt% silver nitrate dissolved in 10 ml double distilled water, and 0.2 g of citric acid and stirred for 2 h. The

entire solution was stirred for 2 h and transferred to an autoclave and calcined at 160 °C for 24 h at a heating rate of 4°/min. The obtained precipitate was centrifuged and repeatedly purified with double distilled water and ethanol multiple times to discard any by-products from the reaction. After purification, NiO/Ag nanocomposite powder was obtained. To remove the traces of water, the purified powder was evacuated at vacuum for 2 h before further analysis. The obtained nanoparticles were sensitive to light and air, the composite was stored in argon-filled glove box for long time use.

2.4. Characterization details

The crystal structure of the prepared nano composites were analyzed using PXRD analysis. The PXRD experiments were carried out by D5000 diffractometer, Siemens, USA with Cu K_α ($\lambda = 1.5406$ Å) radiation and operated with 40 kV and 30 mA. The analyses were carried out between 20 and 80° with step size of 0.02° along with the scan rate of 0.5 s/step. The sizes of the nanoparticles were calculated using the Scherrer equation and complemented by TEM analysis. X-ray photoelectron spectroscopy (XPS) was utilized to study the surface composition of nanomaterials and oxidation of elements present in nanocomposite. The XPS measurements were carried out using Scientific Escalab 250Xi spectrometer with monochromated Al K_α = 1486.68 eV radiation along with the spot size of 650 μm. The XPS spectra of samples were carried out with 20 eV radiation. The binding energies were manually referenced with C 1 s value of adventious carbon with a value of 284.6 eV. The XPS analysis was conducted using Casa XPS software. The particle size of nanocomposites was analyzed by TEM micrographs. The micrographs were taken by FEI TITAN G^2 Titan microscopes operated at 300 keV. The samples were sonicated in ethanol and dispersed in copper grids. The particles were assumed as spherical and calculations were carried out. The samples were in nanosize and surface area was calculated using Micromeritics ASAP 2020 porosimeter. The samples were subjected to high vaccum at 120 °C for 2 h prior to analysis. The band gap of synthesized Ag nanocomposites was derived from UV analysis. The UV measurements were conducted using the Shimadzu UV-3600 UV/Visible spectrometer. The samples were blended with UV-grade barium sulphate, and the reflectance was measured. The reproducibility of all the analysis was examined by repeating experiments for at least three times and error with in the acceptable limit (±5%).

2.5. Photocatalyst testing

All the prepared three nanocomposites were photocatalytically active and analyzed using representative color dye methyl orange and representative colorless dye-4 chlorophenol. The samples were in the aqueous solution and visible radiation was used to carry out the degradation. The visible light source of photocatalytic performance was analyzed using solar simulator SCIENCETECH of AM 1.5 G filter. The degradation studies were followed using UV–Visible spectral analysis and the spectrum was obtained using Perkin Elmer Lambda 35 spectrometer. The photocatalysis reaction suspensions were prepared using 500 ml methyl orange or chlorophenol solution with the concentration of 50 mg/L. After the preparation of the reaction solution 1 g/L of nanocomposite was added. The reaction solution was agitated before irradiation under dark condition to establish adsorption and desorption equilibrium. The resultant reaction solution was aqueous suspension and irradiated with the visible light under constant stirring. The reaction environments were maintained at room temperature to avoid thermal assistance in photocatalytic degradation. For the time dependent analysis of degradation, the samples were collected at regular intervals of time. Before UV analysis, the samples were centrifuged and filtered to avoid any residual floating catalytic particulates. The degradation was followed using 464 nm peak for methyl orange and 223 nm and 280 nm for 4-chlorophenol respectively. The decrease in the corresponding peak intensity is used as a measure of the degradation. The degradation was expressed as percentage using $\eta = (1 - C/C_0) \times 100$, where C_0 is the concentration of before degradation and C is the concentration after the degradation of methylene blue or 4-chlorophenol.

3. Result and discussion

3.1. TEM analysis of nanocomposite

The Ag/metal oxide nanocomposite shape, morphology and crystal structure were analyzed using TEM analysis. TEM analysis showed that the composite consists of small Ag particles attached with the bigger metal oxide nanoparticles (Fig. 1). Representatively, Fig. 1c′ undoubtedly exhibit Ag nanoparticles deposited on the TiO_2 nanoparticles surface and both Ag and TiO_2 nanoparticles are nearly spherical shape. All the metal Ag and metal oxide particles were nearly spherical in nature. The composite aggregated and formed the cluster of Ag and metal oxide nanoparticles. Due to electron density differences, the bright phases are metal oxide nanoparticles and dark phases are Ag nanoparticles. Through HRTEM analysis, through lattice spacing, it was found that small particles are Ag and larger particles are the metal oxides. In the ZnO/Ag sample, TEM micrograph showed that ZnO particles have 10 nm and the Ag particles has 6 nm. In the HRTEM, ZnO nanoparticles were identified thought the (1 0 1) plane with a d value of 2.48 Å and Ag nanoparticles were identified through the (1 1 1) plane with a d value of 2.35 Å. The clear lattice fringes indicated the single crystalline nature of the composite. In the NiO/Ag sample, TEM micrograph showed that NiO particles have 20 nm and the Ag particles has 10 nm. In HRTEM, NiO nanoparticles were identified through the (220) plane with a d value of 1.47 Å and Ag nanoparticles were identified through the (1 1 1) plane with a d value = 2.35 Å. The clear lattice fringes indicated the single crystalline nature of the composite. In the TiO_2/Ag sample, TEM micrograph showed that TiO_2 particles have 8 nm and the Ag particles has 4 nm. In HRTEM, TiO_2 nanoparticles were identified through the (1 0 1) plane (d value = 3.52 Å) and Ag nanoparticles were identified through the (1 1 1) plane (d value = 2.35 Å). The clear lattice fringes indicated the single crystalline nature of the composite. The interfacial planes and lattice mismatch between Ag and metal oxide remains unclear at present and will be explored in near future. In summary, TEM and HRTEM confirmed the crystal structure, shapes of the nanocomposite and composite formation between Ag and metal oxide nanoparticles.

3.2. PXRD analysis of nanocomposite

PXRD analysis has been utilized to confirm the crystal structure of prepared ZnO/Ag, NiO/Ag and TiO_2/Ag nanoparticles. The XRD image of ZnO/Ag, NiO/Ag and TiO_2/Ag nanocomposites were displayed in Fig. 1a, b, c respectively. In the image, silver peaks are identified and represented in orange color separately. The PXRD has shown the combined spectra of metal and metal oxide crystal structures (Fig. S1). The ZnO nanoparticles had hexagonal crystal structure with JCPDS card number 079-02098 and the crystal parameters are a = b = 3.225 Å; c = 5.201 Å. The (1 0 1) plane of ZnO exhibited dominance in the PXRD pattern of ZnO/Ag nanocomposite. The NiO nanoparticles had cubic crystal structure with JCPDS card number 47-1049 and the crystal parameters are a = 4.188 Å. The (2 0 0) plane of NiO exhibited dominance in the PXRD pattern of NiO/Ag nanocomposite. The TiO_2 nanoparticles had tetrahedral crystal structure with JCPDS card number 21-1272 and the crystal parameters are a = b = 3.783 Å; c = 9.531 Å. The (1 0 1) plane of TiO_2 exhibited dominance in the PXRD pattern of TiO_2/Ag nanocomposite. All ZnO/Ag, NiO/Ag and TiO_2/Ag nanocomposites had silver crystal structure of cubic with JCPDS card number 89-3722.

It is to be noted that any new peak or shift in the peaks of metal oxides are not observed in the PXRD analysis (Figs. 2 and S1). The relative intensity of Ag and metal oxide peaks did not alter during composite

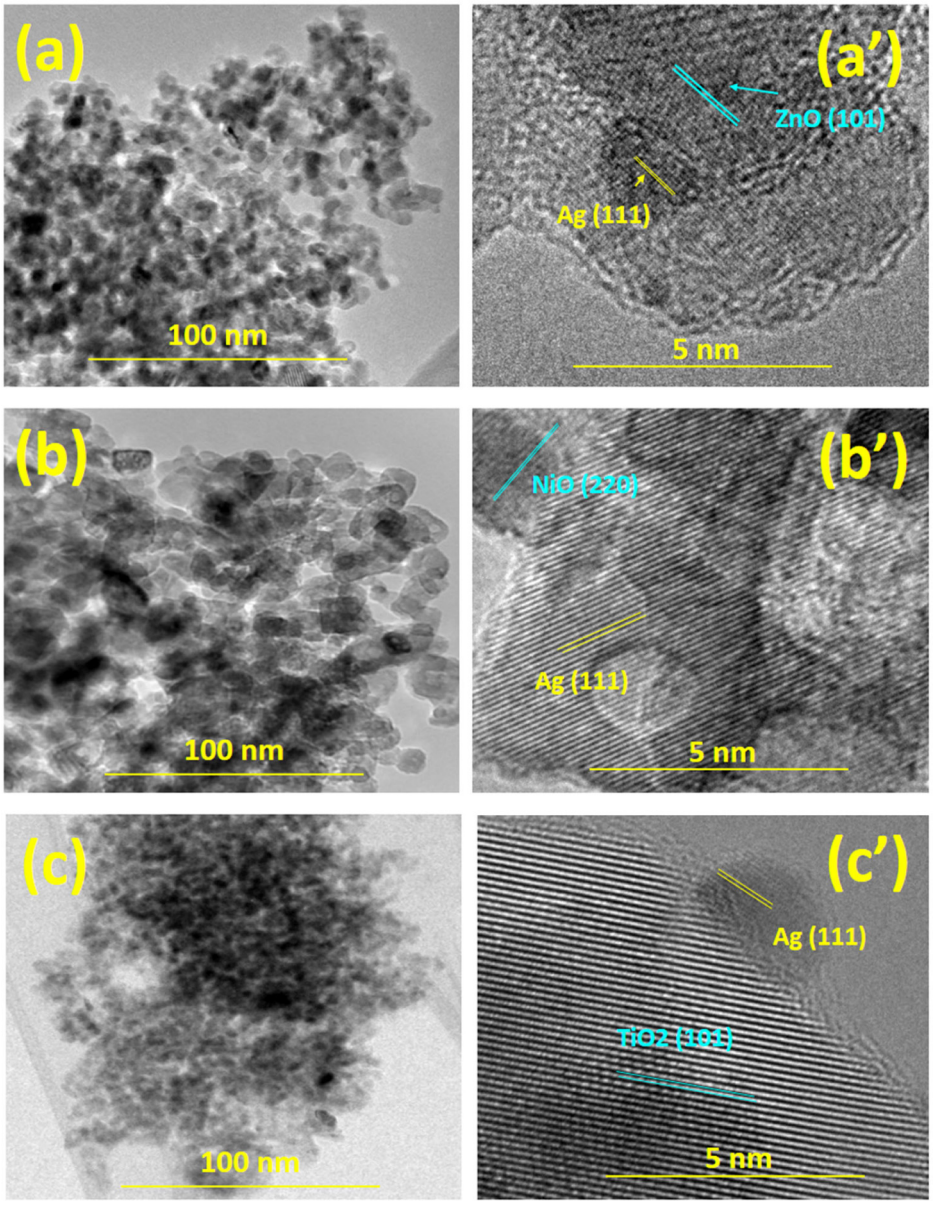

Fig. 1. (a) TEM micrographs of ZnO/Ag aggregated nanocomposites. (a′) High resolution TEM image of ZnO/Ag nanocomposites. (b) TEM micrographs of NiO/Ag nanocomposites. (b′) High resolution TEM image of NiO/Ag nanocomposites. (c) TEM micrographs of TiO_2/Ag nanocomposites. (c′) High resolution TEM image of TiO_2/Ag nanocomposites.

formation. When compared with pure metal oxide formation, nanocomposite peaks are similar which can be attributed to that silver did not incorporated in to the crystal lattice of the metal oxides. Hence it is clear that Ag integration of the composite did not alter the crystal structure of metal oxides or Ag doped with metal oxides. Cho et al. explained that the composite formation of Ag with metal oxide was due to large ionic radii of Ag ion which cannot penetrate the metal oxide with small ionic lattice [50]. Hence from the PXRD patterns, it is concluded that Ag metallic phase was effectively grown on the surface of all the three metal oxides. Since, the Ag and all metal oxides have distinct diffraction peaks, the composite nature of prepared nanocomposite were confirmed. The PXRD analysis was used to identify the average nanoparticle size by Scherrer formula (Table 1). The particle sizes were considered as spherical and the sizes were calculated accordingly. The sizes of the particles were 18, 30, 12 nm for ZnO/Ag, NiO/Ag and TiO_2/Ag respectively. Along with TEM and PXRD studies duly confirmed the crystal structure and Ag composite formation.

3.3. XPS analysis of nanocomposite

The XPS analysis is performed to explore the surface composition and oxidation state of the elements present in the Ag and metal oxide nanocomposite. In Fig. 3, first row represents ZnO/Ag nanocomposites. The Zn, Ag and O profiles are observed in the surface of the nanocomposites. The Zn spectrum consists of two peaks at 1043.3 and 1020.3 eV and attributed to the Zn $2p_{1/2}$ and Zn $2p_{3/2}$ respectively. The difference between two peaks is 23 eV and it was attributed to 2+ oxidation state of Zinc. The Ag spectrum had two peaks at 373.8 and 367.8 eV and assigned to the Ag $3d_{3/2}$ and Ag $3d_{5/2}$ respectively. The difference between two peaks is 6 eV and could be attributed to 0 oxidation state of silver. The oxygen spectrum consists of one peak at 527.8 eV and attributed to the O 1s electron. Notably, the shoulder at the O 1s peak represents the OH radical. It is to be mentioned that the growth of Ag on ZnO did not modify the chemical states of the ZnO nanoparticles when compared to pure ZnO. The results also confirmed

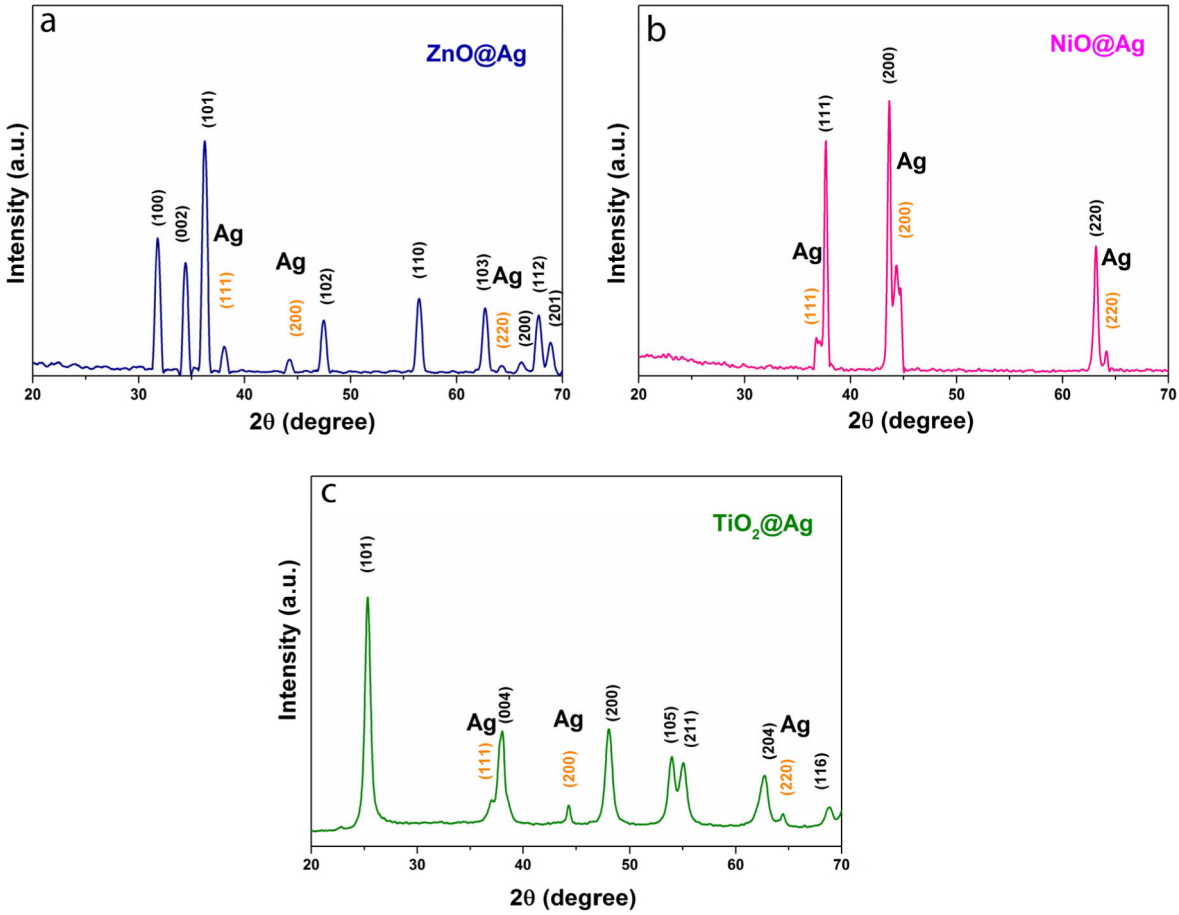

Fig. 2. PXRD analysis (a) Observed patterns of ZnO/Ag nanocomposites. (b) Observed patterns of NiO/Ag nanocomposites (c) Observed patterns of TiO_2/Ag nanocomposites.

that there are no other Ag oxidation state existed in the Ag nanoparticles. Hence both ZnO and Ag existed with own identity in ZnO/Ag nanocomposites.

In Fig. 3, second row represents NiO/Ag nanocomposites. We could observe the Ni, Ag and O profiles in the surface of the nanocomposites. The Ni spectrum consists of two peaks at 853.3 and 871.7 eV and assigned to the Ni $2p_{3/2}$ and Ni $2p_{1/2}$ respectively. The difference between two peaks is 18.4 eV and it attributed to 2+ oxidation state of nickel. The Ag spectrum had two peaks at 373.4 and 367.4 eV and assigned to the Ag $3d_{3/2}$ and Ag $3d_{5/2}$ respectively. The difference between two peaks is 6 eV and could be attributed to metallic silver. The oxygen spectrum consists of one peak at 527.9 eV and attributed to O 1 s electron. It is to be mentioned that the growth of Ag on NiO did not modify the chemical states of the NiO nanoparticles when compared to pure NiO. The results also confirmed that there are no other Ag oxidation state existed in the Ag nanoparticles. Hence both NiO and Ag existed with own identity in NiO/Ag nanocomposites.

In Fig. 3, third row represents TiO_2/Ag nanocomposites. We could observe the Ti, Ag and O profiles in the surface of the nanocomposites. The Ti spectrum consists of two peaks at 456.8 and 462.5 eV and was attributed to Ti $2p_{3/2}$ and Ti $2p_{1/2}$ respectively. The calculated difference between two peaks is 5.7 eV and it was attributed to 4+ oxidation state of titanium. The Ag spectrum consists of two peaks at 373.7 and 367.7 eV and attributed to the Ag $3d_{3/2}$ and Ag $3d_{5/2}$ respectively. The difference between two peaks is 6 eV and could be attributed to 0 oxidation state of silver. The oxygen spectrum consists of one peak at 529.4 eV and attributed to the O 1s electron. It is to be mentioned that, the growth of Ag on TiO_2 did not modify the chemical states of the TiO_2 nanoparticles when compared to pure TiO_2. The results also confirmed that there are no other Ag oxidation state existed in the Ag nanoparticles. Hence both TiO_2 and Ag existed with own identity in TiO_2/Ag nanocomposites.

In summary, XPS analysis showed that Ag in the nanocomposites existed in the metallic form (Ag^0). In the oxides, zinc, nickel, titanium

Table 1
The measured properties of Ag/Metal oxide composites.

S. no	Pure metal oxide surface area of ($m^2.g^{-1}$)	Composite metal oxide/Ag surface area of ($m^2.g^{-1}$)	Band gap (eV)	AVG crystalline size (nm)	TEM predicted size (nm)
1.	58.0 (ZnO)	56.0 (ZnO/Ag)	2.87 (ZnO/Ag)	18 (ZnO/Ag)	Ag = 6 ZnO = 10
2.	34.0 (NiO)	30.2 (NiO/Ag)	2.95 (NiO/Ag)	30 (NiO/Ag)	Ag = 10 NiO = 20
3.	74.0 (TiO_2)	68.2 (TiO_2/Ag)	2.78 (TiO_2/Ag)	12 (TiO_2/Ag)	Ag = 4 TiO_2 = 8

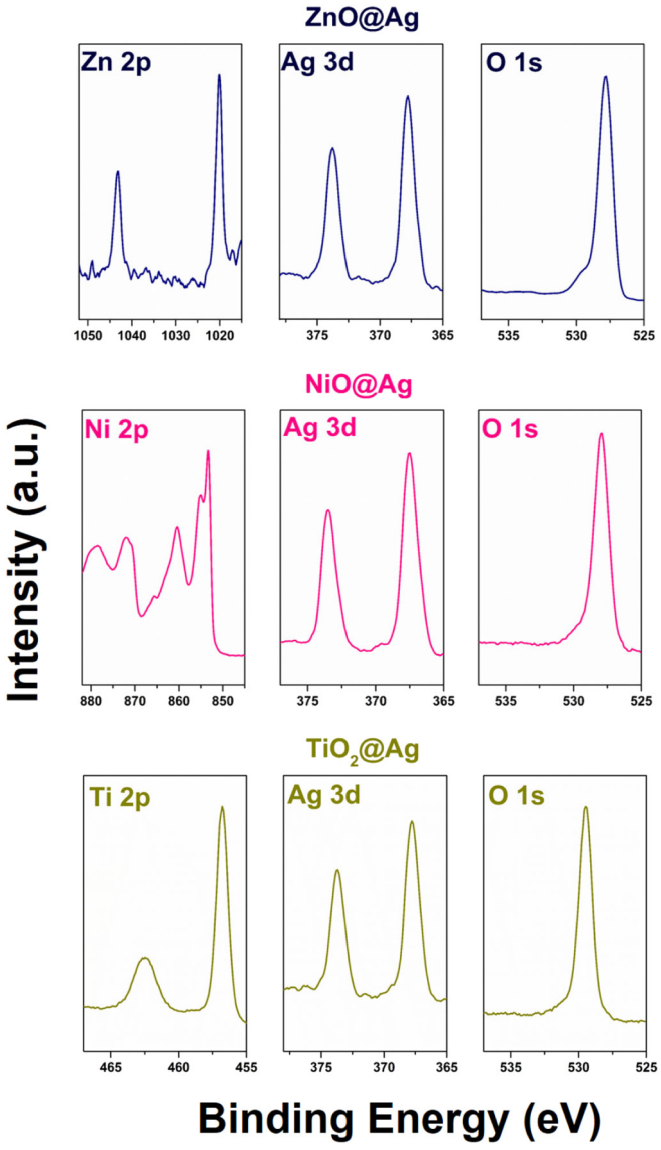

Fig. 3. XPS signature of prepared nanoparticles. First row represents ZnO/Ag nanoparticles. Second row represents NiO/Ag nanoparticles. Third row represents TiO_2/Ag nanoparticles.

existed in the 2+, 2+ and 4+ respectively. As predicted by XRD, metal oxides existed in ZnO, NiO and TiO_2. The XPS results duly confirmed the formation of the composite structure and successful synthesis of nanocomposites.

3.4. BET analysis of nanocomposite

The specific surface area of the prepared nanoparticle was predicted using Brunauer Emmett Teller (BET) method and described in Table 1. The pure ZnO has the surface of 58.0 m^2g^{-1} and Ag integration of ZnO had 56.0 m^2g^{-1}. The pure NiO has the surface of 34.0 m^2g^{-1} and Ag integration of NiO had 30.2 m^2g^{-1}. The pure TiO_2 has the surface of 74.0 m^2g^{-1} and Ag integration of TiO_2 had 68.20 m^2g^{-1}. From the Table 1, it is clear that surface area was not much influenced by Ag integration. Due to agglomeration of nanocomposite particles, the surface area was not influenced by Ag integration. Among the prepared composites, TiO_2 has more surface area and ideal for surface dependent application. The more surface may be attributed to the high Ag content when compared to other NiO and ZnO. Hence, the prepared nanocomposites were in the nano regime and ideal for the photocatalytic degradation process.

3.5. UV analysis

The effect of Ag deposition is observed on metal oxides band gap through the Differential reflectance spectroscopy (DRS) surface analysis (Fig. 4, Table 1). The absorption distribution region of the irradiation is a crucial part in photocatalysts even irrespective of the quantum yield. As expected, all three metal oxides were absorbed in the visible region and red shift (higher wave length) is predicted in the band gap of the metal oxides. The band gap of ZnO/Ag nanoparticles is identified as 2.87 eV, NiO/Ag = 2.95 eV and TiO_2/Ag = 2.78 eV. It is to be noted that pure metal oxides have wide band gap ZnO = 3.2 eV, NiO = 3.6 eV and TiO_2 = 3.2 eV [51,52]. The modification of band gap was assigned to the Ag deposition on the surface of the metal oxides nanoparticles. The nanocomposite materials showed longer wavelength due to SPR phenomenon. The strong interfacial coupling between (TiO_2, ZnO and SnO_2) and the adjoining Ag in metallic state. The rich electrons occupying in the Ag are transferred to (TiO_2, ZnO and SnO_2) which is the reason behind the red-shift [18].

Hence, undoubtedly, the integration of silver into the metal oxide system modifies the band gap from ultra violet region to the visible region. This observation also duly confirmed that Ag is anchored on the surface metal oxides by TEM micrographs. It should be noted that Ag Plasmonic peak is not observed due to the surface dampening by metal oxide nanoparticles. The metal oxide nanoparticles interact with the surface of Ag dampen the Plasmons on the surfaces. The band gap shifts from UV to visible region also validated the proof that silver has the interaction with the metal oxide nanoparticles. In summary, the Ag integration on metal oxides nanoparticles shift the band gap to the visible region and tuned the nanocomposite suitable for the photocatalytic degradation.

4. Degradation of pollutants

The photocatalytic response of the synthesized Ag/metal oxide nanocomposites were examined through the degradation of methyl orange (MO) and 4-chloro phenol (4CP). Since the absorption tuned to visible region, visible light is used for the degradation process. The MO dye is chosen as colorful representative dye and 4CP is used as colorless

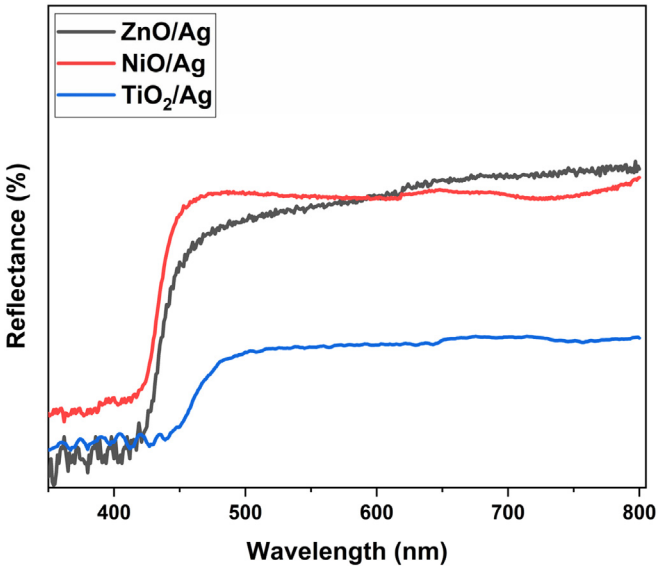

Fig. 4. DRS spectrum of the prepared nanocomposites. We analyzed optical properties based on the influence of Ag integration in metal oxides.

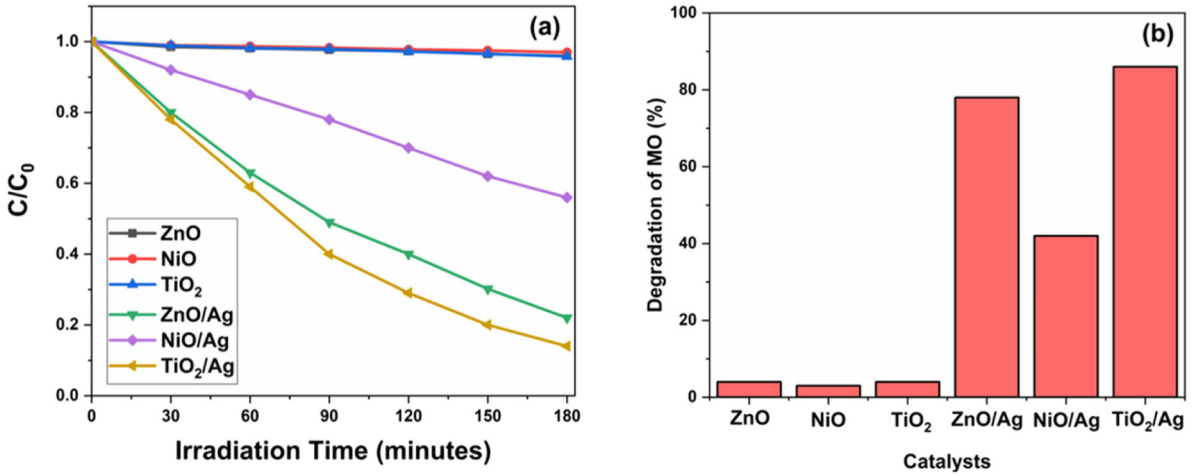

Fig. 5. Degradation of the methyl orange using prepared nanocomposites. (a) Time dependent degradation process of methyl orange with all three nanocomposites where C is absorption peak intensity and C_0 initial absorption peak intensity (b) Comparison of performance of All three nanocomposites. TiO_2/Ag nanocomposite showed the effect performance among the prepeared nanocomposites.

representative pollutant. The MO degradation results were exhibited in Fig. 5 and 4CP degradation results in Fig. 6. In the degradation analysis, y axis was plotted by C/C_0 where C is the absorption peak intensity and C_0 is the initial absorption peak intensity. X axis was plotted with irradiation time of the reaction solution. The degradation has been followed till 3 h with constant intervals of 30 min sampling.

4.1. Degradation of methyl orange

Methyl orange dye was degraded with all ZnO/Ag, NiO/Ag and TiO_2/Ag nanocomposites (Fig. 5). The degradation was followed at 464 nm peak of dye absorption spectra and the peak intensity was decreased with the time along with discoloration. To establish the effectiveness of Ag integration, the control experiments were performed using pure metal oxides under visible light (Fig. 5a). The pure metal oxides as observed did not have any photocatalytic response under the visible light and no discoloration was occurred (<5%). After the silver integration with ZnO, NiO and TiO_2, we observed considerable photocatalytic activity and methyl orange degradation (Fig. 5b). The ZnO/Ag nanocomposite has degraded 78% methyl orange in 180 min duration. The NiO/Ag nanocomposite has degraded 42% methyl orange in 180 min duration. The MO degradation was gradual and constant degradation was observed. The TiO_2/Ag nanocomposite has degraded 86% methyl orange in 180 min duration. The degradation was almost had linear response with the irradiation time. Among all three Ag/metal oxide nanocomposites, TiO_2/Ag has an effective performance with respect to degradation time and MO concentration also which hold superior degradation rate comparable with previous reports [53,54]. The reason behind the high performance of TiO_2/Ag nanocomposite is due to the high surface area 68.2 $m^2.g^{-1}$ when compared to ZnO/Ag (56.0 $m^2.g^{-1}$) and NiO/Ag (30.2 $m^2.g^{-1}$). As expected, due to surface area, ZnO/Ag is having better performance than the NiO/Ag. It should be noted that the absorption capability of different metal oxide/Ag were different and it could also contribute to photocatalytic performance. In summary, the prepared metal oxide/Ag nanocomposites had photocatalytic activity and degraded the MO and among all the nanocomposites, TiO_2/Ag had high performance.

4.2. Degradation of 4-chlorophenol

The methyl orange is a colorful dye and colorant toxic chemicals in textile industry. Similarly, 4-chorophenol is a colorless toxic chemical

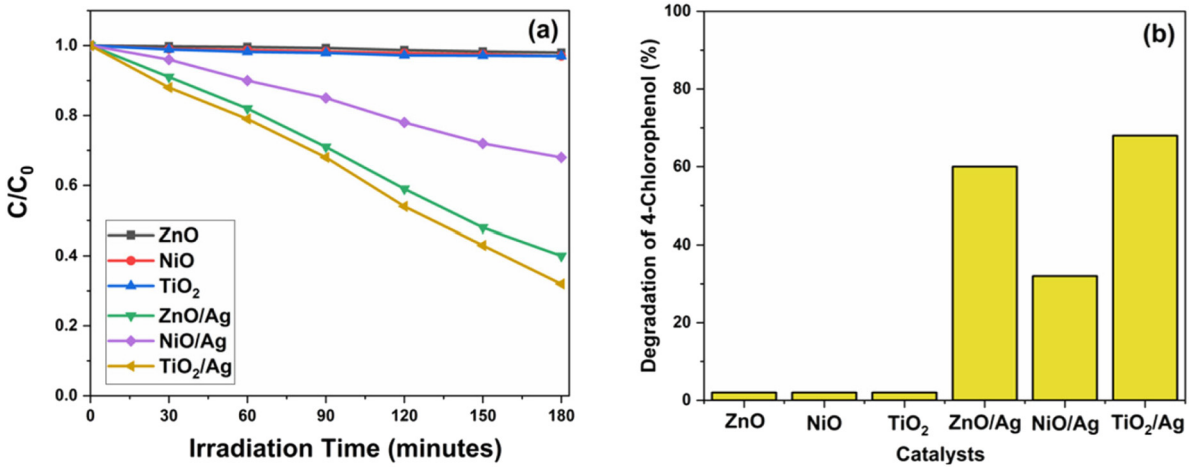

Fig. 6. Degradation of the 4-chlorophenol using prepared nanocomposites. (a) time dependent degradation of 4-chlorophenol with all three nanocomposites where C is absorption peak intensity and C_0 initial absorption peak intensity (b) Comparison of performance of All three nanocomposites. TiO_2/Ag nanocomposite showed the effect performance among the prepared nanocomposites.

and subjected to photocatalytic degradation with prepared Ag/metal oxide composites. The 4-chlorophenol was degraded with all ZnO/Ag, NiO/Ag and TiO_2/Ag nanocomposites (Fig. 5). The degradation was followed at 223 and 280 nm peaks of 4CP absorption spectra and the peak intensity was decreased with the time along with discoloration. To establish the effectiveness of Ag integration, the control experiments were performed using pure metal oxides under visible light (Fig. 6a). As observed, the pure metal oxides did not have any photocatalytic activity under visible light and less 4CP degradation was observed (<5%). After the silver integration with ZnO, NiO and TiO_2, considerable photocatalytic activity was observed and 4CP degradation (Fig. 6b). The degradation was almost had linear response with the irradiation time. The ZnO/Ag nanocomposite has degraded 60% 4CP in 180 min duration. The NiO/Ag nanocomposite has degraded 32% 4CP in 180 min duration. The TiO_2/Ag nanocomposite degraded 68% 4CP in 180 min duration. Among all three Ag/metal oxide nanocomposites, TiO_2/Ag has effective performance with respect to degradation time and 4CP concentration at the end. The reason behind the high performance of TiO_2/Ag nanocomposite was due to high surface area 68.2 $m^2.g^{-1}$. when compared to ZnO/Ag (56.0 $m^2.g^{-1}$) and NiO/Ag (30.2 $m^2.g^{-1}$). As expected, due to surface area, ZnO/Ag is having better performance than NiO/Ag. It should be noted that absorption capability of different metal oxide/Ag were different and it could also contribute to photocatalytic performance. In summary, the prepared metal oxide/Ag nanocomposites had photocatalytic activity and degraded the 4CP and among all the nanocomposites, TiO_2/Ag had high performance.

In summary, performance of the degradation was with respect to the subjected toxic chemicals methyl orange and 4-chlorophenol. The methyl orange has degraded effectively by Ag/metal oxide composite in the photocatalytic degradation process. The methyl orange exhibited the high-performance over 4-chlorophenol due to its simple structure.

4.3. Mechanism of degradation

The mechanism describing electrons-hole population generation is depicted in Fig. 7. In this method, metal Ag and semiconductor metal oxides (ZnO, NiO, TiO_2) were composited each other. Such a specific combination, metal and metal oxide interface are created which establish Schottky barrier [17,18]. The fermi levels of Ag and metal oxide (ZnO, NiO, TiO_2) combine to form new equilibrium Fermi level. During the visible light irradiation, the collective electrons are shifted from new fermi level to conduction band of metal oxides via surface Plasmon which increase the photoelectron population. The photoelectrons promote the degradation process of methyl orange and 4-chlorophenol in the visible region. Hence, plasmonic Ag photocatalytic mechanism dominated over the semiconductor metal oxide photocatalysis. The nanoscale nature of Ag/metal oxide composite provides more surface area and more interfaces which offered more oxygen vacancies. Hence both Ag integration and nanoscale nature of the composites synergistically increase the effectiveness of the photocatalyst by more photoelectron creation. The degradation process was started with photo absorption by Ag/metal oxide nanocomposite (equation in Fig. 8). The absorption process promotes the electrons from valence band to the conduction band in the metal oxides. The photogenerated electron initiate the degradation process. The photogenerated electron reduce the oxygen and forms the $O_2^{\bullet -}$ radical. Then, the radical has reacted with H^+ ions present in the solution and forms $HO_2^{\bullet}$. Then the generated $HO_2^{\bullet}$ radicals combined to form H_2O_2 molecule. The H_2O_2 reacted with $O_2^{\bullet -}$ radical and forms $OH^{\bullet}$ radical. The $OH^{\bullet}$ radical is important active species and degrade the methyl orange and 4-chlorophenol. The entire degradation process of both methyl orange and 4-chlorophenol described in Fig. 8 with the support of GC–MS outcomes. The $OH^{\bullet}$ generation was evident in all Ag/metal oxides nanocomposites which degrade the methyl orange and 4-chlorophenol.

5. Conclusion

In this report, the degradation enhancement is possible by tuning the TiO_2 by Ag nanoparticles. The generality of the method was established by tuning the ZnO and NiO absorption spectra from UV region to the visible region. The materials were completely characterized by PXRD, HRTEM, UV, BET and XPS analysis. The TEM and PXRD studies confirmed the crystal structure and composite formation. TEM micrographs clearly showed that Ag nanoparticle has grown on the surface of metal oxide nanoparticles. The XPS analysis proved that both TiO_2 and Ag existed with own identity in TiO_2/Ag nanocomposites without any new state of elements. Through UV analysis, the band gap of ZnO/Ag = 2.87 eV, NiO/Ag = 2.95 eV and TiO_2/Ag = 2.78 eV and all band gaps were notably shifted to visible region due to new Ag and metal oxide interface. BET analysis explained that agglomeration of

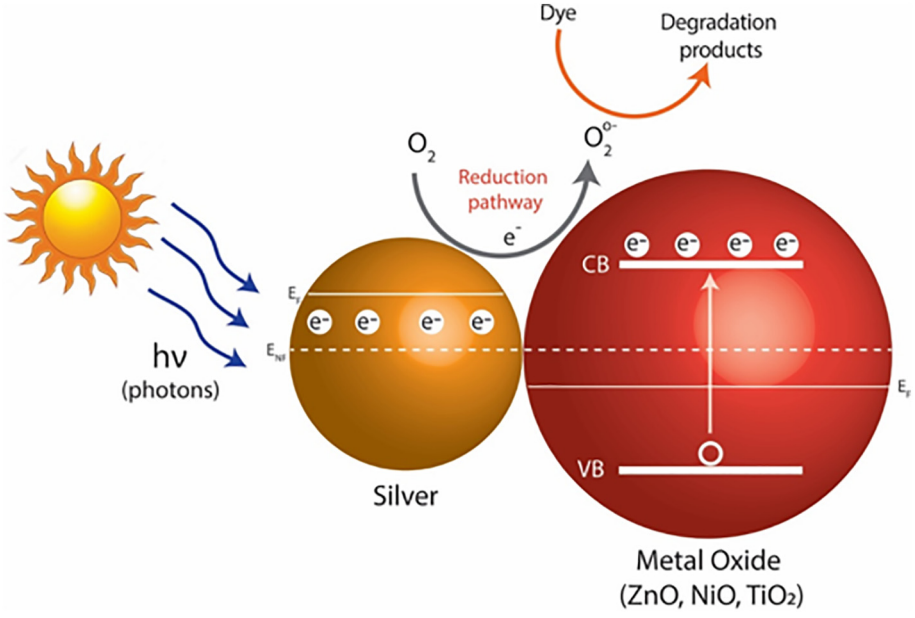

Fig. 7. Schematic diagram of Ag/metal oxide nanocomposites. The silver nanoparticles influence the band gap of metal oxide and assisted the charge carrier generation.

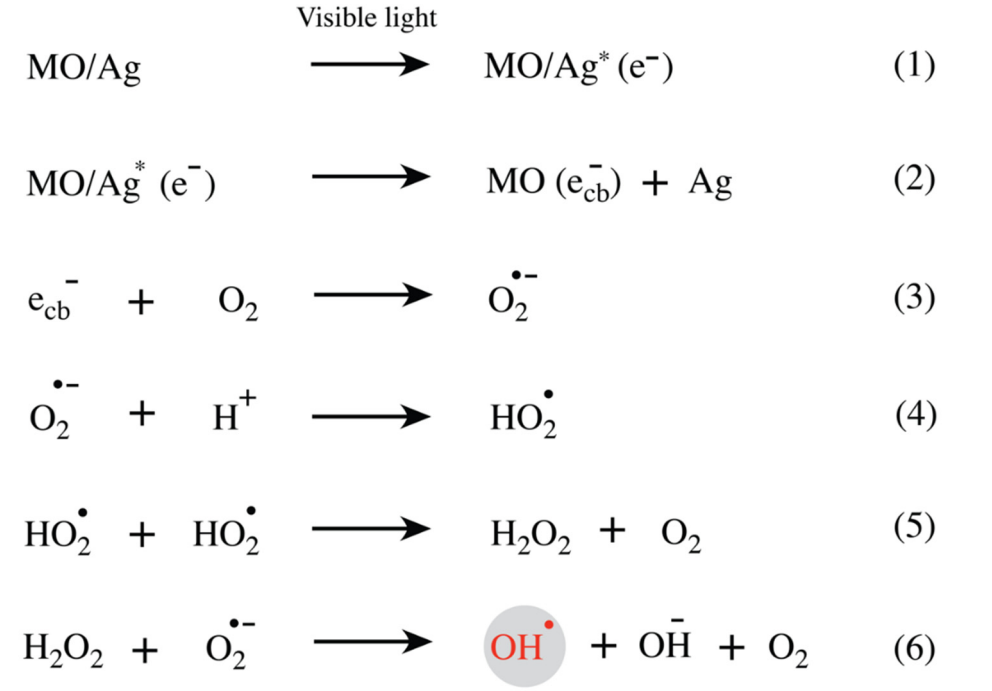

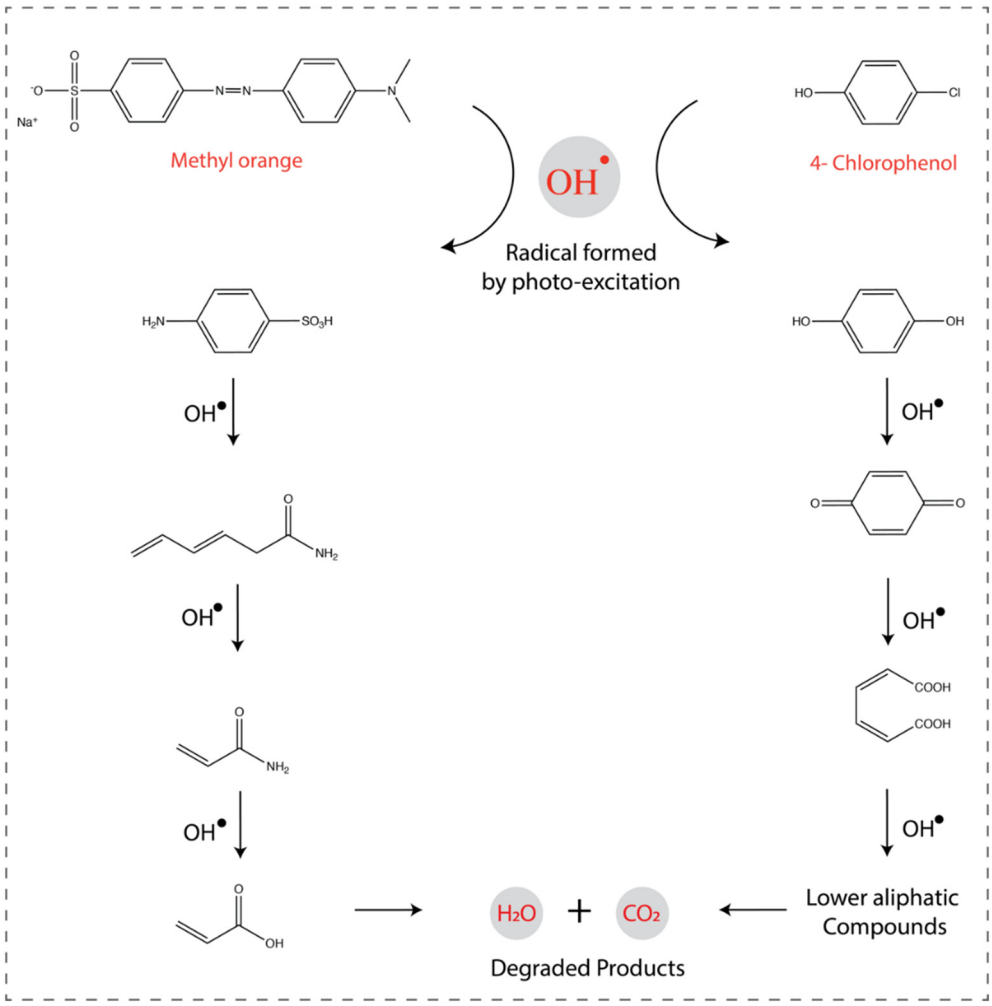

Fig. 8. Schematic diagram of degradation pathway of methyl orange and 4-chlorophenol. The OH free radical generated in photoreaction of catalyst and OH radical was initiated and conducted the degradation.

nanocomposite particles occurred and the surface area was not influenced by Ag integration. Among the prepared composites, TiO_2 has more surface area and ideal for surface dependent photocatalytic degradation. All TiO_2/Ag, NiO/Ag and ZnO/Ag nanocomposites were subjected to photocatalytic degradation under visible light irradiation and degraded the colorful methyl orange and colorless toxic 4-chlorophenol. Among the three, TiO_2/Ag exhibited best performance than ZnO/Ag and NiO/Ag with both methyl orange and 4-chlorophenol. This enhancement of photocatalytic activity is due to Plasmons assistance and nanoscale of catalyst.

Declaration of competing interest

The authors declare no conflict of interest.

Acknowledgment

The authors (S.R., F.G.) acknowledge the support of ANID through the project ANID/FONDAP/15110019. The author (S.R) acknowledge FONDECYT Government of Chile (Project No.: 11170414), for the support to carry out this project.

Appendix A. Supplementary data

Supplementary data to this article can be found online at https://doi.org/10.1016/j.molliq.2020.113588.

References

[1] J.C. Sousa, A.R. Ribeiro, M.O. Barbosa, M.F.R. Pereira, A.M. Silva, A review on environmental monitoring of water organic pollutants identified by EU guidelines, J. Hazard. Mater. 344 (2018) 146–162.
[2] L. Andrade, J. O'Dwyer, E. O'Neill, P. Hynds, Surface water flooding, groundwater contamination, and enteric disease in developed countries: a scoping review of connections and consequences, Environ. Pollut. 236 (2018) 540–549.
[3] M. Baghayeri, B. Mahdavi, Z. Hosseinpor-Mohsen Abadi, S. Farhadi, Green synthesis of silver nanoparticles using water extract of Salvia leriifolia: antibacterial studies and applications as catalysts in the electrochemical detection of nitrite, Appl. Organomet. Chem. 32 (2018), e4057. .
[4] H. Karimi-Maleh, C.T. Fakude, N. Mabuba, G.M. Peleyeju, O.A. Arotiba, The determination of 2-phenylphenol in the presence of 4-chlorophenol using nano-Fe_3O_4/ionic liquid paste electrode as an electrochemical sensor, J. Colloid Interface Sci. 554 (2019) 603–610.
[5] H. Karimi-Maleh, F. Karimi, S. Malekmohammadi, N. Zakariae, R. Esmaeili, S. Rostamnia, M.L. Yola, N. Atar, S. Movagharnezhad, S. Rajendran, An amplified voltammetric sensor based on platinum nanoparticle/polyoxometalate/two-dimensional hexagonal boron nitride nanosheets composite and ionic liquid for determination of N-hydroxysuccinimide in water samples, J. Mol. Liq. (2020) 113185.
[6] M. Baghayeri, B. Maleki, R. Zarghani, Voltammetric behavior of tiopronin on carbon paste electrode modified with nanocrystalline Fe50Ni50 alloys, Mater. Sci. Eng. C 44 (2014) 175–182.
[7] M. Baghayeri, M. Rouhi, M.M. Lakouraj, M. Amiri-Aref, Bioelectrocatalysis of hydrogen peroxide based on immobilized hemoglobin onto glassy carbon electrode modified with magnetic poly (indole-co-thiophene) nanocomposite, J. Electroanal. Chem. 784 (2017) 69–76.
[8] E. Haramoto, M. Kitajima, A. Hata, J.R. Torrey, Y. Masago, D. Sano, H. Katayama, A review on recent progress in the detection methods and prevalence of human enteric viruses in water, Water Res. 135 (2018) 168–186.
[9] P. Movalli, O. Krone, D. Osborn, D. Pain, Monitoring contaminants, emerging infectious diseases and environmental change with raptors, and links to human health, Bird Study 65 (2018) S96–S109.
[10] A. Gogoi, P. Mazumder, V.K. Tyagi, G.T. Chaminda, A.K. An, M. Kumar, Occurrence and fate of emerging contaminants in water environment: a review, Groundw. Sustain. Dev. 6 (2018) 169–180.
[11] R. Narayan, Use of nanomaterials in water purification, Mater. Today 13 (2010) 44–46.
[12] A. Fujishima, X. Zhang, Titanium dioxide photocatalysis: present situation and future approaches, CR CHIM 9 (2006) 750–760.
[13] H. Choi, M.G. Antoniou, M. Pelaez, A.A. De la Cruz, J.A. Shoemaker, D.D. Dionysiou, Mesoporous nitrogen-doped TiO_2 for the photocatalytic destruction of the cyanobacterial toxin microcystin-LR under visible light irradiation, Environ. Sci. Technol. 41 (2007) 7530–7535.
[14] S. Banerjee, S.C. Pillai, P. Falaras, K.E. O'shea, J.A. Byrne, D.D. Dionysiou, New insights into the mechanism of visible light photocatalysis, J. Phys. Chem. Lett. 5 (2014) 2543–2554.
[15] S. Rajendran, M.M. Khan, F. Gracia, J. Qin, V.K. Gupta, S. Arumainathan, Ce^{3+}-ion-induced visible-light photocatalytic degradation and electrochemical activity of ZnO/CeO_2 nanocomposite, Sci. Rep. 6 (2016), 31641. .
[16] R. Saravanan, H. Shankar, T. Prakash, V. Narayanan, A. Stephen, ZnO/CdO composite nanorods for photocatalytic degradation of methylene blue under visible light, Mater. Chem. Phys. 125 (2011) 277–280.
[17] R. Saravanan, N. Karthikeyan, S. Govindan, V. Narayanan, A. Stephen, Photocatalytic degradation of organic dyes using ZnO/CeO_2 nanocomposite material under visible light, Adv. Mat. Res., Trans Tech Publ (2012) 381–385.
[18] R. Saravanan, N. Karthikeyan, V. Gupta, E. Thirumal, P. Thangadurai, V. Narayanan, A. Stephen, ZnO/Ag nanocomposite: an efficient catalyst for degradation studies of textile effluents under visible light, Mater. Sci. Eng. C 33 (2013) 2235–2244.
[19] S.N. Ahmed, W. Haider, Heterogeneous photocatalysis and its potential applications in water and wastewater treatment: a review, Nanotechnology 29 (2018), 342001. .
[20] W. Hou, S.B. Cronin, A review of surface plasmon resonance-enhanced photocatalysis, Adv. Funct . Mater. 23 (2013) 1612–1619.
[21] S. Aftab, N.K. Bakirhan, O. Esim, A. Shah, A. Savaser, Y. Ozkan, S.A. Ozkan, NH2-fMWCNT-titanium dioxide nanocomposite based electrochemical sensor for the voltammetric assay of antibiotic drug nadifloxacin and its in vitro permeation study, J. Electroanal. Chem. 859 (2020), 113857. .
[22] K. Ozturk, N.K. Bakirhan, S.A. Ozkan, B. Uslu, Effect of catalytically active zinc oxide-carbon nanotube composite on sensitive assay of desloratadine metabolite, Electroanalysis 32 (2020) 50–58.
[23] H.G. Bilgicli, H. Burhan, F. Diler, K. Cellat, E. Kuyuldar, M. Zengin, F. Sen, Composites of palladium nanoparticles and graphene oxide as a highly active and reusable catalyst for the hydrogenation of nitroarenes, Microporous Mesoporous Mater. 296 (2020), 110014. .
[24] B. Demirkan, S. Bozkurt, A. Şavk, K. Cellat, F. Gülbağca, M.S. Nas, M.H. Alma, F. Sen, Composites of bimetallic platinum-cobalt alloy nanoparticles and reduced graphene oxide for electrochemical determination of ascorbic acid, dopamine, and uric acid, Sci. Rep. 9 (2019) 1–9.
[25] S. Malekmohammadi, H. Hadadzadeh, Z. Amirghofran, Preparation of folic acid-conjugated dendritic mesoporous silica nanoparticles for pH-controlled release and targeted delivery of a cyclometallated gold (III) complex as an antitumor agent, J. Mol. Liq. 265 (2018) 797–806.
[26] S. Malekmohammadi, H. Hadadzadeh, H. Farrokhpour, Z. Amirghofran, Immobilization of gold nanoparticles on folate-conjugated dendritic mesoporous silica-coated reduced graphene oxide nanosheets: a new nanoplatform for curcumin pH-controlled and targeted delivery, Soft Matter 14 (2018) 2400–2410.
[27] Z. Shamsadin-Azad, M.A. Taher, S. Cheraghi, H. Karimi-Maleh, A nanostructure voltammetric platform amplified with ionic liquid for determination of tert-butylhydroxyanisole in the presence kojic acid, Journal of Food Measurement and Characterization 13 (2019) 1781–1787.
[28] F. Wang, Q. Li, D. Xu, Recent progress in semiconductor-based nanocomposite photocatalysts for solar-to-chemical energy conversion, Adv. Energy Mater. 7 (2017), 1700529. .
[29] H. Karimi-Maleh, O.A. Arotiba, Simultaneous determination of cholesterol, ascorbic acid and uric acid as three essential biological compounds at a carbon paste electrode modified with copper oxide decorated reduced graphene oxide nanocomposite and ionic liquid, J. Colloid Interface Sci. 560 (2020) 208–212.
[30] S. Rajendran, D. Manoj, K. Raju, D.D. Dionysiou, M. Naushad, F. Gracia, L. Cornejo, M. Gracia-Pinilla, T. Ahamad, Influence of mesoporous defect induced mixed-valent NiO (Ni^{2+}/Ni^{3+})-TiO_2 nanocomposite for non-enzymatic glucose biosensors, Sensors Actuators B Chem. 264 (2018) 27–37.
[31] J. Mohanraj, D. Durgalakshmi, R.A. Rakkesh, S. Balakumar, S. Rajendran, H. Karimi-Maleh, Facile synthesis of paper based graphene electrodes for point of care devices: a double stranded DNA (dsDNA) biosensor, J. Colloid Interface Sci. 566 (2020) 463–472.
[32] H. Karimi-Maleh, M. Shafieizadeh, M.A. Taher, F. Opoku, E.M. Kiarii, P.P. Govender, S. Ranjbari, M. Rezapour, Y. Orooji, The role of magnetite/graphene oxide nanocomposite as a high-efficiency adsorbent for removal of phenazopyridine residues from water samples, an experimental/theoretical investigation, J. Mol. Liq. 298 (2020), 112040. .
[33] H. Arzani, M. Adabi, J. Mosafer, F. Dorkoosh, M. Khosravani, H. Maleki, H. Nekounam, M. Kamali, Preparation of curcumin-loaded PLGA nanoparticles and investigation of its cytotoxicity effects on human glioblastoma U87MG cells, Biointerface Research in Applied Chemistry 9 (2019) 4225–4231.
[34] Q. Husain, An overview on the green synthesis of nanoparticles and other nanomaterials using enzymes and their potential applications, Biointerface Research in Applied Chemistry 9 (2019) 4255–4271.
[35] F. Tahernejad-Javazmi, M. Shabani-Nooshabadi, H. Karimi-Maleh, 3D reduced graphene oxide/$FeNi_3$-ionic liquid nanocomposite modified sensor; an electrical synergic effect for development of tert-butylhydroquinone and folic acid sensor, Compos. Part B 172 (2019) 666–670.
[36] T. Hirakawa, P.V. Kamat, Photoinduced electron storage and surface plasmon modulation in Ag@ TiO_2 clusters, Langmuir 20 (2004) 5645–5647.
[37] K. Awazu, M. Fujimaki, C. Rockstuhl, J. Tominaga, H. Murakami, Y. Ohki, N. Yoshida, T. Watanabe, A plasmonic photocatalyst consisting of silver nanoparticles embedded in titanium dioxide, J. Am. Chem. Soc. 130 (2008) 1676–1680.
[38] J. Jiang, L. Zhang, Rapid microwave-assisted nonaqueous synthesis and growth mechanism of AgCl/Ag, and its daylight-driven plasmonic photocatalysis, Chem. Eur. J. 17 (2011) 3710–3717.
[39] J. Lan, X. Zhou, G. Liu, J. Yu, J. Zhang, L. Zhi, G. Nie, Enhancing photocatalytic activity of one-dimensional KNbO 3 nanowires by Au nanoparticles under ultraviolet and visible-light, Nanoscale 3 (2011) 5161–5167.

[40] J. Yu, G. Dai, B. Huang, Fabrication and characterization of visible-light-driven plasmonic photocatalyst Ag/AgCl/TiO_2 nanotube arrays, J. Phys. Chem. C 113 (2009) 16394–16401.
[41] X. Chen, H.Y. Zhu, J.C. Zhao, Z.F. Zheng, X.P. Gao, Visible-light-driven oxidation of organic contaminants in air with gold nanoparticle catalysts on oxide supports, Angew. Chem. Int. Ed. Engl. 47 (2008) 5353–5356.
[42] D.B. Ingram, P. Christopher, J.L. Bauer, S. Linic, Predictive model for the design of plasmonic metal/semiconductor composite photocatalysts, ACS Catal. 1 (2011) 1441–1447.
[43] K. Mori, M. Kawashima, M. Che, H. Yamashita, Enhancement of the photoinduced oxidation activity of a ruthenium (II) complex anchored on silica-coated silver nanoparticles by localized surface plasmon resonance, Angew. Chem. Int. Ed. Engl. 49 (2010) 8598–8601.
[44] W.A. Murray, W.L. Barnes, Plasmonic materials, Adv. Mater. 19 (2007) 3771–3782.
[45] H. Zhang, G. Wang, D. Chen, X. Lv, J. Li, Tuning photoelectrochemical performances of Ag–TiO_2 nanocomposites via reduction/oxidation of Ag, Chem. Mater. 20 (2008) 6543–6549.
[46] P. Wang, B. Huang, X. Qin, X. Zhang, Y. Dai, J. Wei, M.H. Whangbo, Ag@ AgCl: a highly efficient and stable photocatalyst active under visible light, Angew. Chem. Int. Ed. Engl. 47 (2008) 7931–7933.
[47] W. Zhang, X. Yang, Q. Zhu, K. Wang, J. Lu, M. Chen, Z. Yang, One-pot room temperature synthesis of Cu_2O/Ag composite nanospheres with enhanced visible-light-driven photocatalytic performance, Ind. Eng. Chem. Res. 53 (2014) 16316–16323.
[48] D. Lin, H. Wu, R. Zhang, W. Pan, Enhanced photocatalysis of electrospun Ag–ZnO heterostructured nanofibers, Chem. Mater. 21 (2009) 3479–3484.
[49] Y. Zheng, L. Zheng, Y. Zhan, X. Lin, Q. Zheng, K. Wei, Ag/ZnO heterostructure nanocrystals: synthesis, characterization, and photocatalysis, Inorg. Chem. 46 (2007) 6980–6986.
[50] S.A. Ansari, M.M. Khan, M.O. Ansari, J. Lee, M.H. Cho, Biogenic synthesis, photocatalytic, and photoelectrochemical performance of Ag–ZnO nanocomposite, J. Phys. Chem. C 117 (2013) 27023–27030.
[51] S.C. Rai, K. Wang, Y. Ding, J.K. Marmon, M. Bhatt, Y. Zhang, W. Zhou, Z.L. Wang, Piezo-phototronic effect enhanced UV/visible photodetector based on fully wide band gap type-II ZnO/ZnS core/shell nanowire array, ACS Nano 9 (2015) 6419–6427.
[52] A.O. Juma, E.A. Arbab, C.M. Muiva, L.M. Lepodise, G.T. Mola, Synthesis and characterization of CuO-NiO-ZnO mixed metal oxide nanocomposite, J. Alloys Compd. 723 (2017) 866–872.
[53] H. Wang, J. Niu, X. Long, Y. He, Sonophotocatalytic degradation of methyl orange by nano-sized Ag/TiO_2 particles in aqueous solutions, Ultrason. Sonochem. 15 (2008) 386–392.
[54] H. Chaker, L. Chérif-Aouali, S. Khaoulani, A. Bengueddach, S. Fourmentin, Photocatalytic degradation of methyl orange and real wastewater by silver doped mesoporous TiO_2 catalysts, J. Photochem. Photobiol. A Chem. 318 (2016) 142–149.